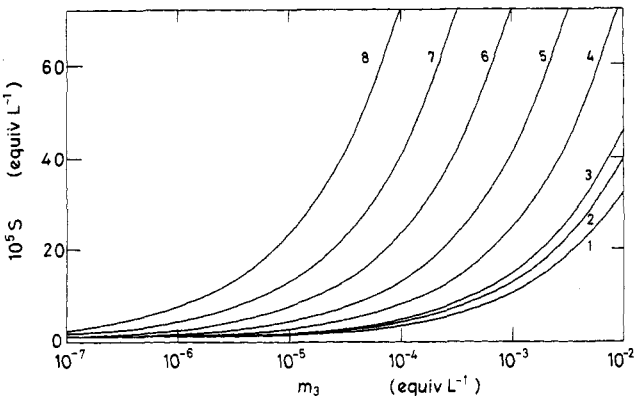

Figure 7. Plots of solubility of 2–1000 type polyelectrolyte complex estimated theoretically against the concentration of foreign salt. Influence of valencies of anionic components of foreign salt. $Z_{2g} = 2$; $Z_{2p} = 1000$; $Z_{3c} = 1$; $Z_{3a} = 1$ (curve 1), 2 (2), 3 (3), 10 (4), 30 (5), 100 (6), 300 (7), 1000 (8); $\xi = 1.5$, $S^* = 1 \times 10^{-6}$ M.

the foreign salt compared with the complex of $\xi = 2.85$ (for typical vinyl-type macroions).

The influence of the valency of the anionic component of the foreign salt on the solubility of 2–1000 type polyelectrolyte complex is shown in Figure 7. Clearly, the foreign salts solubilize more effectively as the valency (Z_{3a}) increases. This is explained reasonably by the fact that the electrostatic shielding effect of foreign salts of high valencies is substantial against the macrocation–macroanion attraction. It should be mentioned here that the use of Manning's theory will not be justified in the strict sense for the polyelectrolyte complex systems with high valencies of counterions because their conformations may deviate from an infinite line charge.

Registry No. NaPES, 25053-27-4; DMCS, 27577-32-8; NaPSS-C5PVP, 114943-71-4; NaCl, 7647-14-5; KCl, 7447-40-7; LiCl, 7447-41-8; polybrene, 28728-55-4.

References and Notes

(1) Bungenberg de Jong, H. G.; Kruyt, H. R. *Kolloid Z.* **1930**, *50*, 39.
(2) Holleman, L. W. J.; Bungenberg de Jong, H. G.; Tjaden Modderman, R. S. *Kolloid-Beih.* **1934**, *39*, 334.
(3) Fuoss, R. M.; Sadek, H. *Science (Washington, D.C.)* **1949**, *110*, 552.
(4) Voorn, M. J. *Recl. Trav. Chim. (Pays-Bas)* **1956**, *75*, 317, 405, 427, 925.
(5) Michales, A. S.; Miekka, R. G. *J. Phys. Chem.* **1961**, *65*, 1765.
(6) Michaels, A. S. *Ind. Eng. Chem.* **1965**, *57*, 32.
(7) Vogel, M. K.; Cross, R. A.; Bixler, H. J.; Guzman, R. J. *J. Macromol. Sci. Chem.* **1970**, *A4*, 675.
(8) Tsuchida, E.; Osada, Y.; Sanada, K. *J. Polym. Sci., A1* **1972**, *10*, 3397.
(9) Nakajima, A.; Sato, H. *Biopolymers* **1972**, *11*, 1345.
(10) Zezin, A. B.; Rogacheva, V. B.; Kabanov, V. A.; Kargin, V. A. *Vysokomol. Soedin., Ser. A* **1972**, *14*, 772.
(11) Pal, M. K.; Ghosh, A. K. *Makromol. Chem.* **1973**, *169*, 273.
(12) Tsuchida, E.; Osada, Y. *Makromol. Chem.* **1974**, *175*, 593.
(13) Sato, H.; Nakajima, A. *Colloid Polym. Sci.* **1974**, *252*, 294.
(14) Lohman, T. M.; De Haseth, P. L.; Records, M. T., Jr. *Biophys. Chem.* **1978**, *8*, 281.
(15) Cundall, R. B.; Lawton, J. B.; Murray, D. *Makromol. Chem.* **1979**, *180*, 2913.
(16) Kabanov, A.; Papisov, N. M. *Vysokomol. Soedin., Ser. A* **1979**, *21*, 243.
(17) Duszeln, J.; Martin, V.; Klein, J. *Makromol. Chem.* **1979**, *180*, 255.
(18) Domard, A.; Rinaudo, M. *Macromolecules* **1980**, *13*, 898.
(19) Okubo, T.; Hongyo, K.; Enokida, A. *J. Chem. Soc., Faraday Trans. 1* **1984**, *80*, 2087.
(20) Dautzenberg, H.; Dautzenberg, H. *Acta Polym.* **1985**, *36*, 102.
(21) Manning, G. S. *J. Chem. Phys.* **1969**, *51*, 924.
(22) Manning, G. S. *Polyelectrolytes*; Selegny, E., Ed.; Reidel: Dordrecht, Holland, 1974.
(23) Manning, G. S. *J. Chem. Phys.* **1969**, *51*, 924.
(24) Kozak, D.; Kristan, J.; Dolar, D. *Z. Phys. Chem.* **1971**, *76*, 85.
(25) Kozak, D.; Dolar, D. *Z. Phys. Chem.* **1971**, *76*, 93.
(26) Wells, J. D. *Biopolymers* **1973**, *12*, 223.
(27) Oman, S.; Dolar, D. *Z. Phys. Chem.* **1967**, *56*, 1, 13.
(28) Dolar, D.; Leskovsek, H. *Makromol. Chem.* **1968**, *118*, 60.
(29) Manning, G. S. *J. Chem. Phys.* **1969**, *51*, 934.
(30) Dixler, D. S.; Ander, P. *J. Phys. Chem.* **1973**, *77*, 2684.
(31) Kowlansky, A.; Sasso, R.; Spagnuola, V.; Ander, P. *Macromolecules* **1977**, *10*, 78.
(32) Skerjanc, J. *J. Phys. Chem.* **1973**, *77*, 2225.
(33) Ise, N.; Okubo, T. *Macromolecules* **1978**, *11*, 439.
(34) Mita, K.; Okubo, T. *J. Chem. Soc., Faraday Trans. 1* **1974**, *70*, 1546.
(35) Mita, K.; Okubo, T.; Ise, N. *J. Chem. Soc., Faraday Trans. 1* **1975**, *71*, 1932.
(36) Vesnaver, G.; Rudez, M.; Pohar, C.; Skerjanc, J. *J. Phys. Chem.* **1984**, *88*, 2411.
(37) Mita, K.; Kunugi, S.; Okubo, T.; Ise, N. *J. Chem. Soc., Faraday Trans. 1* **1975**, *71*, 936.
(38) Mita, K.; Okubo, T.; Ise, N. *J. Chem. Soc., Faraday Trans. 1* **1976**, *72*, 1033.
(39) Manning, G. S. *Biopolymers* **1972**, *11*, 937, 951.
(40) Harada, S.; Arai, K. *Makromol. Chem.* **1967**, *107*, 78.
(41) Negi, Y.; Harada, S.; Ishizuka, O. *J. Polym. Sci.* **1967**, *5*, 1951.
(42) Hildebrand, F. B. *Introduction to Numerical Analysis*; McGraw-Hill: New York, 1956.

Microdomains in Poly(4-methylpentene-1) Single Crystals

P. Pradère, J.-F. Revol, and R. St. John Manley*

Pulp and Paper Research Institute of Canada, Department of Chemistry, McGill University, 3420 University Street, Montreal, PQ, Canada H3A 2A7.

Received October 23, 1987

ABSTRACT: It is shown that in a given single crystal of poly(4-methylpentene-1) (P4MP1) polymorph III there exist narrowly delimited microdomains that give rise to different electron diffraction patterns. These domains have the same crystallographic unit cell but opposite *c* axis (chain axis) orientation. Dark field electron microscope images show that the number, size, and shape of the microdomains vary from one crystal to another. The domain boundaries are usually perpendicular to one crystal edge. These effects are discussed in relation to twinning by merohedry.

The presence of domains having different crystallographic orientation is well-known in twinned polymer crystals.[1,2] However, apart from this special case, polymer single crystals are generally considered to be structurally homogeneous. Here we report that single crystals of poly(4-methylpentene-1) (P4MP1) contain narrowly delimited microdomains that give rise to different electron diffraction patterns. The location and shape of these domains have been precisely defined by diffraction con-

* To whom correspondence should be addressed.

0024-9297/88/2221-2747$01.50/0

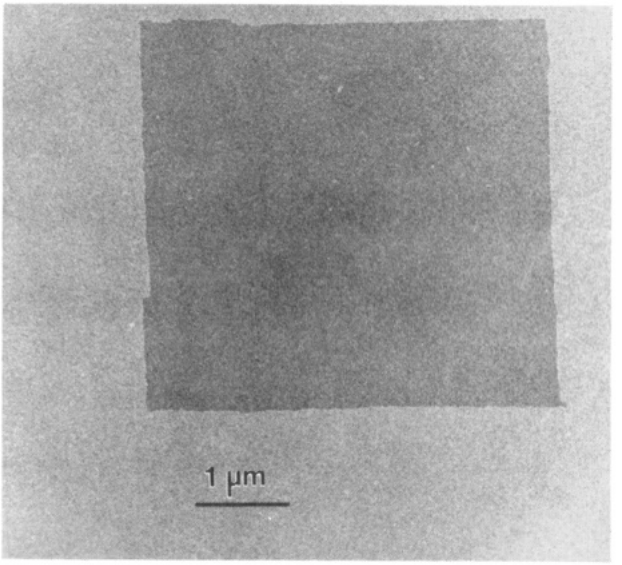

Figure 1. Bright field image of a P4MP1 single crystal grown at 60 °C in xylene (not shadowed). Ninety percent of the crystals observed have lateral dimensions of 4–5 μm.

trast imaging in the dark field mode.

P4MP1 single crystals were prepared from a commerical ICI sample having an isotactic content estimated at more than 95%. The intrinsic viscosity [η] in decalin at 135 °C is 2.8 dL/g, which corresponds to M_v = 350 000.[3,4] Single crystals of polymorphs I and III were prepared from dilute solutions (polymer concentration <0.05%) in sealed glass tubes. Polymorph III was obtained either by isothermal crystallization in xylene or by slow cooling of a solution in an equivolume mixture of xylene–cyclohexane (cooling rate lower than 10 °C/h) from the dissolution temperature (135 °C) to room temperature according to the method described by Charlet and Delmas.[5] Polymorph I was obtained by slow cooling of a hexadecane solution (dissolution temperature 185 °C). Crystals suspended in the solvent were deposited on carbon-coated electron microscope grids (carbon thickness ~100 Å), and the solvent was allowed to evaporate at ambient temperature.

The crystals were examined at 120 kV with a Philips EM 400T electron microscope (side entry goniometer) equipped with a liquid nitrogen anticontamination trap and a Philips PW 6587 low-dose unit. As is well-known, organic materials are strongly susceptible to radiation damage so that the crystallinity is rapidly destroyed under the electron beam.[6] Consequently, the illumination conditions were carefully chosen in order to image the crystals before their destruction. The total end point dose (TEPD) of the crystals was measured by observing the fading of the electron diffraction pattern under a defined illumination. Beam current density on the sample was measured with the help of a chart, provided by Philips, giving the screen current as a function of the plate exposure time indicated on the microscope. A TEPD of 27 C/m^2 (1.7 e$^-$/Å^2) was found at 120 kV so that P4MP1 is more sensitive than polyethylene (TEPD of about 100 C/m^2).

Electron diffraction patterns were obtained either by means of the classical technique of selected area diffraction or by concentrating the beam with the condensor lens in conjunction with the use of a small condensor aperture and spot size. The latter technique allows the electron diffraction pattern to be obtained from a whole crystal (an area of diameter 5 μm) without irradiating the neighboring crystals. Highly sensitive Kodak DEF-5 X-ray films, used for dark field imaging, were developed 5 min in Kodak X-ray developer and fixed 10 min in standard Kodak rapid fixer at a temperature of 20 °C.

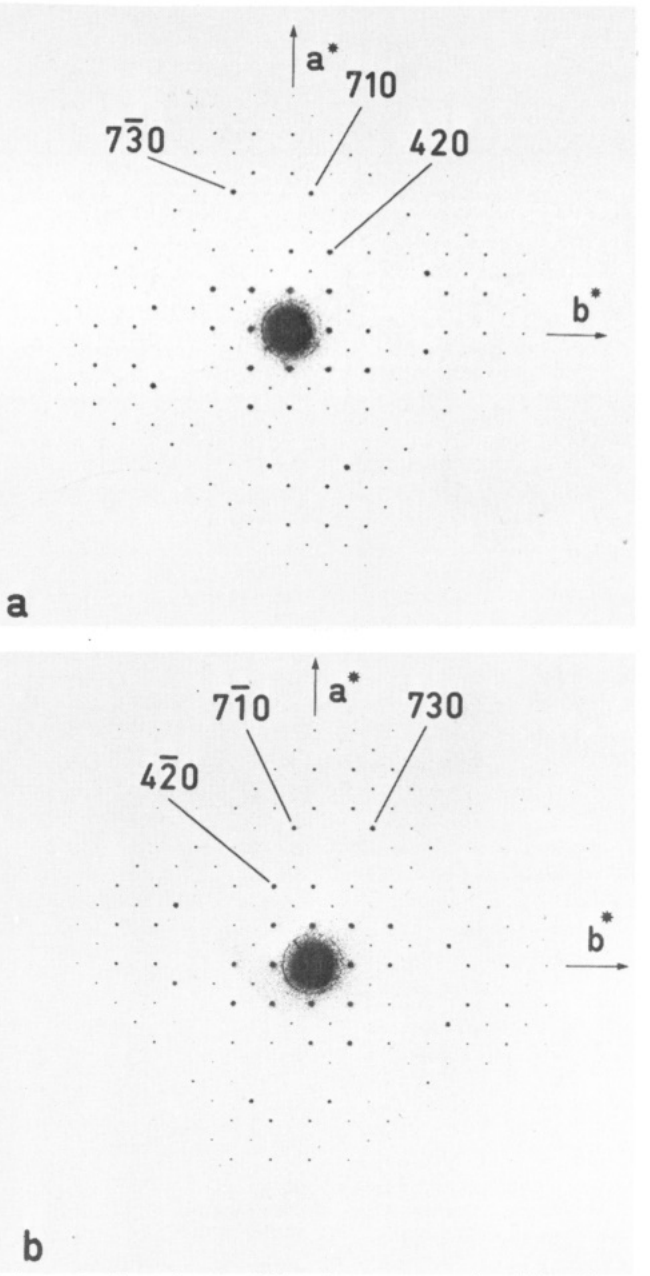

Figure 2. Two electron diffraction patterns related by mirror symmetry obtained at different positions in a given single crystal of P4MP1 form III using a small selector aperture (0.5 μm in diameter). The difference between the two patterns involves two groups of reflections: 420, 710, 7$\bar{3}$0, etc., for (a) and 4$\bar{2}$0, 7$\bar{1}$0, 730, etc., for (b). In (a), reflections of the first group are strong, while reflections of the second group are weak or nonexistant. In (b), the opposite occurs.

Figure 1 shows a typical square-shaped crystal of P4MP1 obtained by isothermal crystallization in xylene at 60 °C. The thickness of the crystals was estimated by shadowing to be 12 nm. When areas of about 0.5-μm diameter are selected by an appropriate aperture to perform electron diffraction, typical patterns like that in Figure 2a are obtained. The indexing of this electron diffraction pattern is consistent with the tetragonal unit cell of the polymorph III characterized in a previous paper[7] with the parameters $a = b = 1.94$ nm. The only symmetry element in the pattern is a 4-fold rotation axis perpendicular to the (a^*,b^*) reciprocal lattice plane and passing through the central spot. An important feature observed with such crystals is that, when different areas are selected by the diffraction

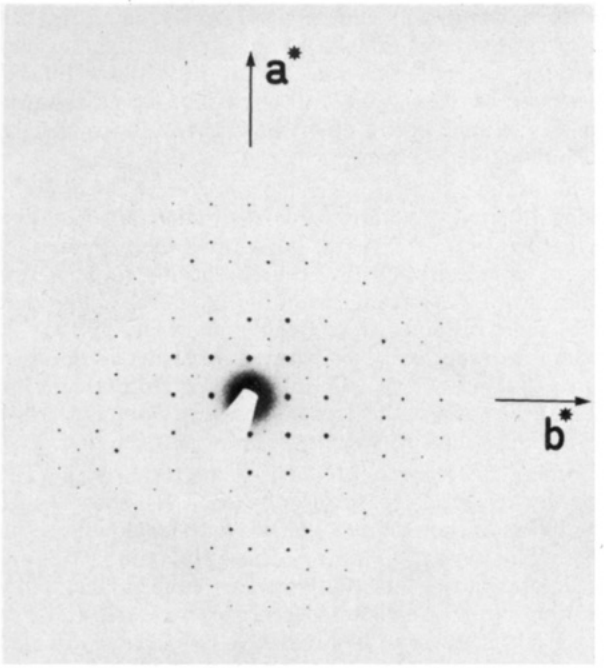

Figure 3. Electron diffraction pattern obtained from a whole crystal (selected area of about 5 μm in diameter) of P4MP1 form III. The pattern exhibits mirror symmetry and can be considered as a mixture of the two patterns of (a) and (b) in Figure 2.

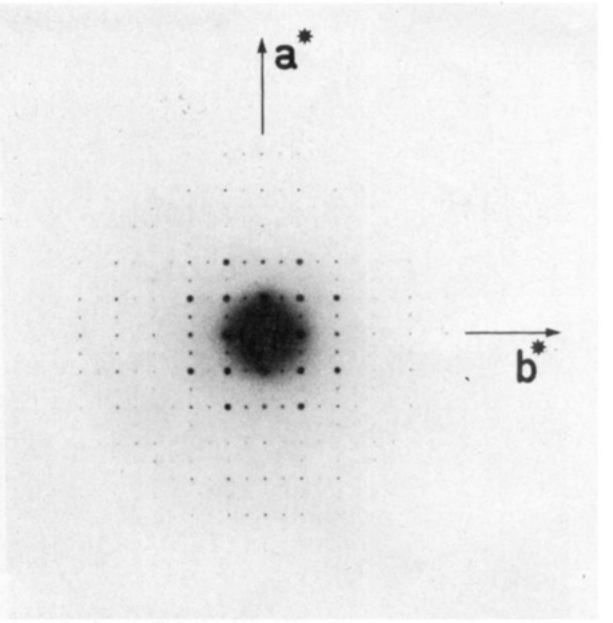

Figure 4. Electron diffraction pattern obtained from a P4MP1 polymorph I crystal. The size of the selected area is about 1 μm in diameter. No difference is observed by selecting different areas in a given crystal, and the overall aspect of the pattern is independent of the dimension of the area selected.

aperture all across a given single crystal, a second diffraction pattern may be obtained as shown in Figure 2b. This second pattern is related to that of Figure 2a by mirror symmetry, the plane of symmetry being perpendicular to the a^*b^* reciprocal lattice plane and parallel to the a^* axis. For example, inspection of Figure 2a shows that the 420 reflection is very strong and the $4\bar{2}0$ is absent or very weak, whereas the reverse occurs in Figure 2b. Similar observations were made with other reflections such as 710, $7\bar{3}0$, $8\bar{2}0$, and $10\bar{2}0$ and their symmetric counterpart with respect to the a^* axis, i.e., $7\bar{1}0$, 730, 820, and 1020. The phenomenon cannot be attributed to slight local variations in the sample orientation. Indeed, the presence of a 4-fold rotation axis perpendicular to the a^*b^* reciprocal lattice plane, and consequently perpendicular to the flat lamellar crystals in real space, implies that the plane of the crystal remains parallel to the plane of observation. In addition, a slight tilt (less than 1 deg) of the specimen in any direction decreases the symmetry of the pattern, as expected, but does not introduce any mirror plane in the pattern. It thus appears that these single crystals are composed of different areas that give an electron diffraction pattern showing either a "left" or "right" 4-fold rotation axis.

When electron diffraction is performed on a whole single crystal, patterns such as that in Figure 3 are produced. This pattern shows reflections up to the 14th order corresponding to a resolution of 0.13 nm. Depending on the crystal, a difference in the relative intensities of the reflections previously mentioned is observed. This difference of intensity is an indication that in a given crystal the domains producing the two patterns in a and b of Figure 2 are not present in equal amounts since otherwise a perfectly symmetrical pattern should have been obtained. In contrast to the crystals of polymorph III, the selected area electron diffraction patterns of polymorph I show additional symmetry elements such as planes of symmetry (see Figure 4), and no structural heterogeneity can be detected.

In order to visualize the two types of domains present in one single crystal of polymorph III, diffraction contrast imaging in the dark field mode was performed using the 420 reflection alone. The closest reflections in the electron diffraction pattern of one crystal (i.e., the 400 and 220 reflections) are separated by only 1.0 nm^{-1}; thus, an objective aperture with a diameter of 5 μm was selected corresponding to 0.8 nm^{-1} in the diffraction plane. The dark field image presented in Figure 5 was obtained by tilting the central beam at an angle corresponding to the 420 Bragg angle and in a direction parallel to the diffraction vector $\vec{g}$ shown on the image. Thus, crystals having their [420] axis approximately parallel to $\vec{g}$ are imaged with the 420 reflection. These crystals are easily recognized since the [420] axis is at an angle of 26° to their edge. Because the spacing of the (400) planes (0.485 nm) is close to that of the (420) planes (0.430 nm), crystals oriented with one edge parallel to the diffraction vector will also be imaged, but with the 400 reflection. Such 400 dark field images (see arrow a in Figure 5) show that the crystals are flat to better than 1.5° according to the calculated kinematical rocking curve. In Figure 5, the crystals imaged with the 420 reflections exhibit white and dark domains. The white domains are those giving rise to electron diffraction patterns that exhibit the strong 420 diffraction spot, whereas the rest of the crystal constitutes domains whose electron diffraction pattern contains the strong $4\bar{2}0$ reflection. These highly contrasted images clearly reveal the presence of two types of domains. The possibility that the white zones result from the superposition of two crystals can be rejected, because when the crystallinity had been totally destroyed after the TEPD was exceeded, the entire crystal showed the same contrast, indicating that the crystal is a monolayer having a constant thickness (Figure 6).

As shown in Figure 5, the general trend is that the boundaries of the domains are well delineated and follow crystallographic lines perpendicular to the closest bounding face of the crystal (see arrow 1). Occasionally however, a domain boundary is parallel to a sector boundary (see arrow 2), and sometimes they are not linear but curved (see arrow 3). Due to the low resolution of such images, esti-

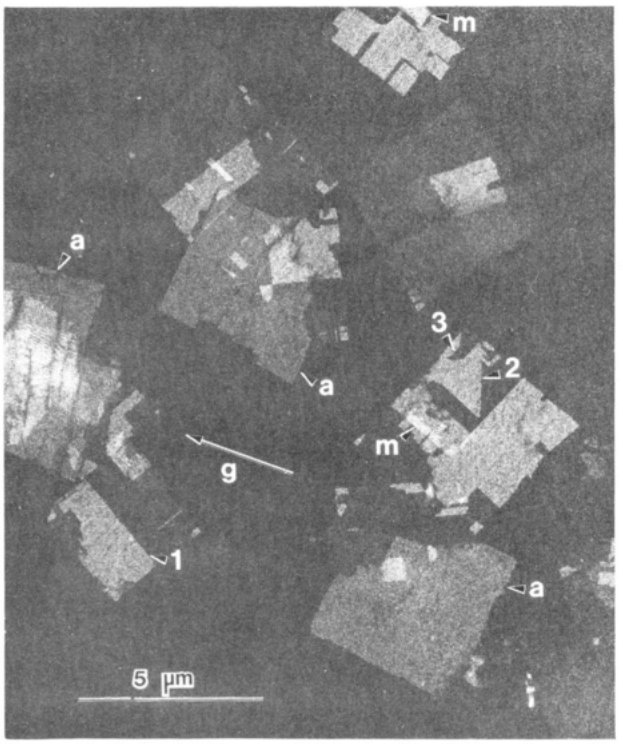

Figure 5. Dark field image obtained with a tilt angle equal to the Bragg angle corresponding to the 420 reflection. Crystals properly oriented toward the diffraction vector $\vec{g}$ (i.e., for which one edge makes an angle of 26° ± 10° with $\vec{g}$) are imaged with the 420 reflection. Crystals with one edge parallel to $\vec{g}$ are imaged with the 400 reflection (arrow a) and show a uniform contrast. Crystals imaged with the 420 reflection show domains and Moiré patterns (arrow m). Domains usually have straight boundaries parallel to one crystal edge (arrow 1) or, less frequently, parallel to a sector boundary (arrow 2). Curved domain boundaries (arrow 3) are also observed in a few cases. Some of the crystals (see those marked a, upper center and lower right) are fractured along two edges.

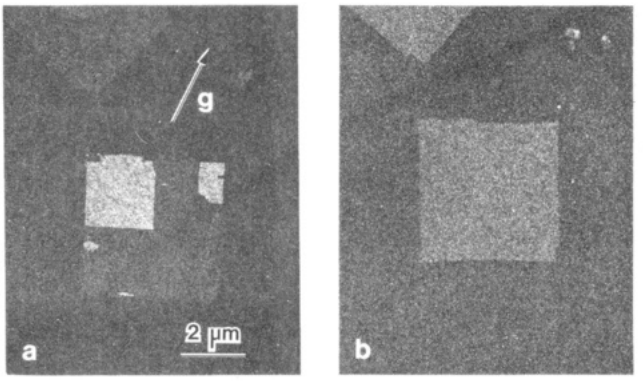

Figure 6. Successive dark field images obtained with the 420 reflection on one P4MP1 form III crystal: (a) undegraded crystal showing domains (diffraction contrast) and (b) after crystallinity destruction; the whole crystal is imaged by amplitude contrast.

mated to be about 20 nm, the possibility that the apparent curved boundaries are "zigzag lines", alternately parallel to one crystal side or to one sector boundary, cannot be ruled out. As seen in Figure 5, the two types of domains are randomly distributed within a given crystal. Their shape is variable, sometimes well defined such as square or rectangular and sometimes ill defined. The domain size is also variable; they can be as small as the resolution limit (about 20 nm) or they can extend over the entire crystal.

As indicated earlier, the electron diffraction patterns from the two different domains are related by mirror symmetry. This means that if one of the domains is turned upside down it will give exactly the same diffraction pattern as the other domain. Thus, the two domains have the same molecular packing in the (a,b) plane but are positioned in the crystal with opposite c axis directions. One way to explain this effect would be in terms of right- and left-handed helices.

The existence, in a given single crystal, of domains having different crystallographic orientation is in fact quite normal in twinned crystals[8] where twinning is generally evident from morphological considerations[9] and the twin domains originate from a common nucleus.[10] The dark field images obtained from P4MP1 show clearly that the domains are randomly distributed and thus do not grow from a single nucleus. Thus, twinning from a common nucleus cannot account for the observed domains. However, other forms of twinning cannot be excluded.

Donnay and Donnay[11] have used the terminology TLS (twin-lattice symmetry) to describe twins that show a single orientation of the reciprocal lattice with single diffraction spots. This type of twinning, where the twin lattice and the crystal lattice are one and the same is also called twinning by merohedry.[12] According to Catti and Ferraris,[13] such twins can be divided in two classes. In class I, the twin-related reflections have equal intensities, and, on an absolute scale, the set of intensities measured on the twin is identical with one that would be measured on a single crystal. In class II, the twin-related reflections differ in intensity, and the intensity of the reflection of a twin is the sum of two reflections which are not equivalent. In the present work, if twinning is the cause of the observed domains, then it is a case of "twinning by merohedy" of class II. The twin operation would be a 2-fold axis of symmetry perpendicular to the c axis, resulting in the occurrence of two orientations of the polar microdomains which would have the same structural features but opposite c axis direction.

It is interesting to compare twinning in poly(ethylene oxide) (PEO) crystals with that observed in the present work. In the growth of PEO single crystals, twinning can be induced by quenching a solution in xylene from 60 to −30 °C.[10] In this way, highly imperfect crystals are formed and subsequent self-seeding gives a preparation containing about 50% twinned crystals, all grown from seeds that conserved the original twinning produced during the quenching process. Under isothermal conditions, however, normal crystallographic growth is preferred to twinning. On the other hand, it is evident from the present work that P4MP1 does not require such a complex procedure to form twinned crystals. Twinning occurs spontaneously during growth at a relatively much higher frequency than is usual for polymer crystals. This indicates that in P4MP1 the energy required to form a twin does not differ substantially from the energy implied in normal growth.

In the present work, it has been possible to demonstrate the presence of microdomains in the polymorph III crystals only because of the particular symmetry of the electron diffraction pattern. As mentioned earlier, this effect cannot be demonstrated in polymorph I crystals because the symmetry of the electron diffraction pattern does not allow local differences in structure to be detected. However, it may be noted that form III crystals can readily be converted into form I by annealing at $T > 72$ °C.[7] In this process the microdomain structure is expected to be conserved. Thus, the form I crystals may contain microdomains even though their electron diffraction pattern does not show local variations. In that case, the phenomenon may be described as being due to "twinning by merohedry" of class I. We leave open the question as to whether similar

effects may occur in other types of polymer single crystals.

Finally, it is worth noting that these observations may be of some importance in crystal structure analysis of polymers. The exact symmetry of a crystal is crucial for the determination of its structure. If the crystals contain microdomains, the X-ray or electron diffraction pattern may contain "mixed" symmetry elements leading to an incorrect crystal structure analysis.

Registry No. P4MP1, 25068-26-2.

References and Notes

(1) Geil, P. H. *Polymer Single Crystals*; Wiley-Interscience: New York, 1963.
(2) Wunderlich, B. *Macromolecular Science*; Academic: New York, 1972; Vol. 1, p 283.
(3) Tani, S.; Hamada, F.; Nakajima, A. *Polymer J. (Tokyo)* **1973**, *5*, 86.
(4) Dong, D. H. M.Sc. Thesis, Université du Québec, Montreal, 1980.
(5) Charlet, G.; Delmas, G. *Polymer* **1984**, *25*, 1619.
(6) See for instance: *Electron Microscopy and Microbeam Analysis*; Siegel, B. M., Ed.; Wiley: New York, 1975.
(7) Charlet, G.; Delmas, G.; Revol, J. F.; Manley, R. St. J. *Polymer* **1984**, *25*, 1613.
(8) Frank, F. C.; Keller, A.; O'Connor, A. *Philos. Mag.* **1964**, *5*, 293.
(9) Blundell, D. J.; Keller, A. *J. Macromol. Sci., Phys.* **1968**, *B2*, 337.
(10) Kovacs, A. J.; Lotz, B.; Keller, A. *J. Macromol. Sci., Phys.* **1969**, *B3*(3), 385.
(11) Donnay, G.; Donnay, J. D. H. *Can. Mineral.* **1974**, *12*, 422.
(12) Friedel, G. *Leçons de Cristallographie*; Berger-Levrault: Paris, 1926.
(13) Catti, M.; Ferraris, G. *Acta Crystallogr., Sect. A: Cryst. Phys., Diffr. Theor. Gen. Crystallogr.* **1976**, *A32*, 163.

Conformational Analysis of Broken Rodlike Chains. 1. Scattering Function of Rods Joined Together by Flexible Coils

Yoshio Muroga

Department of Synthetic Chemistry, Faculty of Engineering, Nagoya University, Furo-cho, Chikusa-ku, Nagoya 464, Japan.

Received November 20, 1987; Revised Manuscript Received February 22, 1988

ABSTRACT: The particle-scattering function for rods joined together by flexible coils is derived by using Hermans' technique, which was originally used for freely hinged rods. It is shown that the scattering function derived can be reduced to that for freely hinged rods and also for randomly coiled chain by changing the content of flexible coils in the particle. Moreover, it is pointed out that the reduced particle scattering function is independent of molecular weight distribution in the high wave vector region, available in small-angle X-ray scattering experiments, so that the reduced particle scattering function may be used for studying the conformation of polypeptides with a broad molecular weight distribution.

Introduction

It is well-known that most polypeptides such as poly(L- or D-glutamate), poly(L-lysine) or DNA show the helix-to-coil transition. A polymer in its helix region is not a rigid rod but may have a structure of freely hinged rods, while that in its helix-to-coil transition region may be represented by several rods joined together by flexible coils. Those structures are sometimes called "broken rods". However, detail in its structures has not yet been clarified. To study the detail in their molecular conformations, the particle-scattering function in light scattering (LS) or small-angle X-ray scattering (SAXS) may be useful. The particle-scattering function for freely hinged rods has been presented by Hermans and Hermans,[1] and the particle-scattering functions of polymers having the conformations of random coil, rigid rod, and wormlike chains[2-5] have already been calculated. However, the particle-scattering function for the broken rod in the helix-to-coil transition region has not been derived.

In the present paper, it is shown that Hermans' technique can be extended to the calculation of the scattering function of a molecule consisting of several rods joined together by flexible coils. Application of the results to analysis of the conformation of poly(sodium D-glutamate) in the helix-to-coil transition region is given in the following paper[6] in this issue.

In general, the particle-scattering function in LS or SAXS is sensitive to molecular weight distribution. However, it is shown that the functional form in the large wave vector region, which can be attained in SAXS, is insensitive to molecular weight distribution since the scattering from only a part of the chain can be observed.

Computation Result

Let $\vec{s}_0$ be the unit vector in the direction of the primary beam, $\vec{s}$ the vector in the direction of the scattered beam, $\vec{r}_{jk}$ the distance vector between the j and k scatterers, and $\tilde{\lambda}$ the wave length of the light in the solution. The wave vector $\vec{h}$ is defined by

$$\vec{h} = 2\pi(\vec{s} - \vec{s}_0)/\tilde{\lambda} \tag{1}$$

The absolute value of $\vec{h}$ is

$$h = (4\pi/\tilde{\lambda}) \sin(\theta/2) \tag{2}$$

where θ is the scattering angle. The scattering intensity is proportional to

$$R_\theta = \sum_j \sum_k \exp[i\vec{h}\cdot\vec{r}_{jk}] \tag{3}$$

As is shown in Figure 1, a rod of length A and a rod of length a are named R rod and C rod, respectively, and all rods are numbered in succession: the first C rod is numbered 1 and the last R rod is numbered $N(n+1)$. Here, let the position of a scatterer in the R rod be denoted by P and that in the C rod by Q. If the position of P in the $k(n+1)$th R rod is measured as a distance between P and the end of the $(k(n+1)-1)$th rod, it is given by the distance $Ax_{k(n+1)}$, where x varies from 0 to 1. When the scatterers are distributed continuously in the rod, the scattering from a scatterer at P should be regarded as that from an element

0024-9297/88/2221-2751$01.50/0